Arabian Journal for Science and Engineering (2023) 48:1031–1040
https://doi.org/10.1007/s13369-022-07293-4

RESEARCH ARTICLE-PHYSICS

# DFT and Molecular Docking Study of 1-(2´-Thiophen)-2-propen-1-one-3-(2,3,5-trichlorophenyl) (TTCP) Molecule as Antiviral to Covid-19 Main Protease

Cengiz Ipek[1] · Hacer Gümüş[2] · Merve Şimşek[3] · Murat Tosun[4]

Received: 10 May 2021 / Accepted: 20 September 2022 / Published online: 27 October 2022


**Abstract**
Thiophene-containing compounds have antiviral properties and may be among the drugs tested for the treatment of COVID-19 diseases. In order to better understand the molecular definition of the 1-(2´-Thiophen)-2-propen-1-one-3-(2,3,5-trichlorophenyl) molecule from thiophene-containing compounds, the physico-chemical (molecular structure analysis, spectroscopic properties, boundary orbital analysis) mechanisms underlying the protein–ligand interaction should be examined in detail. For this reason, geometric parameters, IR and UV–vis spectra, conformational analysis, electronic, NBO and NLO properties, molecular electrostatic potential map and Mulliken charge distributions of the TTCP molecule were investigated theoretically using DFT theory in the Gaussian program. Accordingly, molecular docking calculations with COVID-19 main protease (PDB 5R7Y) were performed to determine the pharmaceutical activities of the TTCP molecule against coronavirus diseases.

**Keywords** Covid-19 · Molecular docking · DFT · UV–vis spectra · Conformational analysis

## 1 Introduction

The coronavirus emerged as a rapidly spreading epidemic in the city of Wuhan, China, in late 2019. An effective antiviral drug has not yet been developed against the SARS-CoV-2 virus, which was named as a global epidemic on March 11, 2020, by the World Health Organization. Rapid and detailed research is ongoing as there is an urgent need to search for effective antiviral agents to combat the COVID-19 virus.

Today, many researches go on in drug design using molecular docking (MD) studies. Protein–ligand interaction studies by molecular docking (MD) play an important role in the knowledge of mechanisms in the discovery, design and development of drugs. Ligand selection in molecular docking is based on their antiviral activity.

The Thiophene-containing compound forms the basic framework for various species in pharmacological, chemical, biological and industrial fields. Thiophene-containing compounds are widely used in polymer electronics [1], non-static covering, electronic and optoelectronic [2, 3] devices, optoelectronic applications [4], petroleum and fossil fuel [5] and modern drug design. Compounds containing thiophene nucleus possess a broad range of biological activities such as anti-inflammatory, analgesic, antifungal, ocular hypertensive activities, and antimicrobial activities [6–8]. In light of this information, TTCP molecule, one of the compounds containing thiophene with antiviral activity, may be among the drugs tested for the treatment of COVID-19 diseases. In order to better understand the molecular definition of the TTCP molecule, first of all, the optimized structures of the molecules were determined using the density functional theory (DFT) method in the Gaussian 09 W program. Using optimized constructs in molecular docking calculations is more precise, making the program more reliable for use in construct-based drug design.

✉ Cengiz Ipek
cengiz.ipek@medeniyet.edu.tr

1 Department of Civil Engineering, Istanbul Medeniyet University, Unalan Campus, Uskudar, 34700 Istanbul, Turkey

2 Kocaeli University, Golcuk Vocational School, Automotive Technology Program , Kocaeli University, Kocaeli, Turkey

3 Department of Physics, Faculty of Arts and Sciences, Sakarya University, 54187 Serdivan, Sakarya, Turkey

4 Mechanical Engineering Department, Faculty of Mechanical Engineering, Istanbul Technical University, 34437 Gumussuyu, Istanbul, Turkey

Manjunath et al. [1] were synthesized TTCP molecule, and its geometric parameters (bond lengths and bond angles) and vibrational spectroscopy were performed experimentally. However, the theoretical studies on above-mentioned analyses for the TTCP molecule are neglected. In order to eliminate this deficiency, we investigated the structural, spectroscopic, conformations and Mulliken charge analysis, molecular electrostatic potential maps, electronic, NLO and NBO properties of TTCP molecule at DFT method. In addition; Molecular docking calculations were performed with COVID-19 main protease (PDB 5R7Y) to determine the pharmaceutical activities of the TTCP molecule against coronavirus diseases.

## 2 Computational Methods

### 2.1 DFT Calculations

The theoretical modeling was calculated for the TTCP molecule by Gaussian 09 software [9] in the ground state. The molecular structure of the optimized molecule was drawn by Gaussian View 5 program [10]. Theoretical calculations of the TTCP molecule performed with B3LYP [11, 12] and HSEh1PBE [13–16] with 6–311++ G(d,p) [17]. UV–vis was performed with TD-HSEh1PBE and TD-B3LYP approach in ground state. Nonlinear optical parameters were calculated at both levels. Natural bond analysis calculations were made to investigate various quadratic interactions [18]. The DFT method also made application to calculate molecular frontier orbital energies and polarizability, as well as molecule charges, molecular docking, and electrostatic potential (MEP) surface.

### 2.2 Molecular Docking Calculations (Ligand and Target Protein Preparation)

Before starting the molecular docking calculations, the 3D molecular structure of COVID-19 (5R7Y) were downloaded from the Protein Data Bank (PDB) of the Structural Bioinformatics Research Laboratory (RCSB) [19]. Thus, the ligand (TTCP) and target (PDB 5R7Y) were determined for molecular docking calculations. Molecular Docking calculations were performed by using the AutoDock Tools (ADT) Version 1.5.6 [20] to find the ligand–protein docking interactions. The PyMOL software package [21] has analyzed the output of the AutoDock (version 4.0) program [22]. In addition, Discovery Studio Visualizer 3.5 software [23] was used to visualize the docked active sites in the protein and its H-bond interactions.

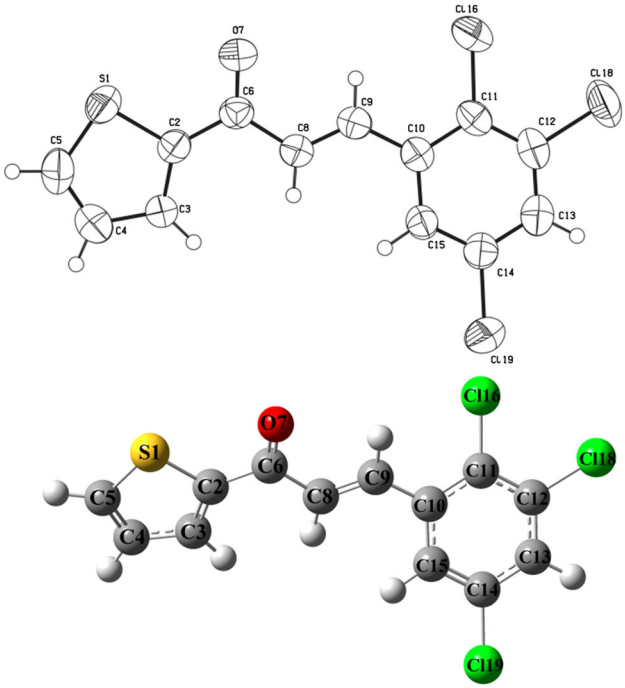


**Fig. 1** Experimental and calculated structure with B3LYP for the TTCP

## 3 Results and Discussion

### 3.1 Geometric Optimization

The TTCP was studied by Manjunath et al. [1]. The unit cell parameters $a = 16.6170(6)$, $b = 7.6180(5)$, $c = 10.9280(11)$ (in Å) $\beta = 104.635°$ and V = 1338.47(17) Å$^3$. The obtained geometric structure is seen in Fig. 1. Obtained geometric data listed in Table 1. In the study, Theoretical bond lengths (for C–C) were found in the range 1.370–1.482 Å and 1.371–1.489 (in Å) at HSEh1PBE and B3LYP, respectively. Experimental bond lengths (C–C) are seen in the range of 1.340 and 1.476 (in Å) [1]. Experimental $C_{11}$–$C_{16}$, $C_5$–$S_1$, and $C_6$–$O_7$ bond lengths are 1.729, 1.689, and 1.226 Å, respectively [1]. Calculated bond lengths were observed as 1.744, 1.723, 1.224 Å for the B3LYP and 1.726, 1.710, 1.220 Å for the HSEh1PBE. THE experimental $C_3$–$C_2$–$S_1$ bond angle is 110.9° [1], and this angle has been seen at 110.8° for the B3LYP and 110.9° for the HSEh1PBE.

$R^2$ (linear correlation coefficients) of calculated bond lengths are 0.9942 for the B3LYP and 0.9934 for the HSEh1PBE. $R^2$ (linear correlation coefficients) of calculated bond angles are 0.9867° for the B3LYP and 0.9850° for the HSEh1PBE. The best calculating geometric data correlation coefficient of the TTCP is obtained with the B3LYP.

**Table 1** Experimental and calculated bond lengths and bond angles

| | Experimental | DFT | |
|---|---|---|---|
| | x-ray | B3LYP | HSEh1PBE |
| *Bond length(Å)* | | | |
| $C_{11}$–$C_{12}$ | 1.385 | 1.399 | 1.396 |
| $C_{11}$–$C_{10}$ | 1.399 | 1.410 | 1.406 |
| $C_{11}$–$Cl_{16}$ | 1.729 | 1.744 | 1.726 |
| $C_{12}$–$C_{13}$ | 1.380 | 1.391 | 1.388 |
| $C_{12}$–$Cl_{18}$ | 1.734 | 1.745 | 1.727 |
| $C_{13}$–$C_{14}$ | 1.377 | 1.389 | 1.386 |
| $C_{14}$–$C_{15}$ | 1.367 | 1.384 | 1.382 |
| $C_{14}$–$Cl_{19}$ | 1.738 | 1.753 | 1.735 |
| $C_{15}$–$C_{10}$ | 1.405 | 1.403 | 1.398 |
| $C_{10}$–$C_9$ | 1.459 | 1.466 | 1.460 |
| $C_9$–$C_8$ | 1.318 | 1.341 | 1.339 |
| $C_8$–$C_6$ | 1.476 | 1.489 | 1.482 |
| $C_6$–$O_7$ | 1.226 | 1.224 | 1.220 |
| $C_6$–$C_2$ | 1.461 | 1.472 | 1.466 |
| $C_2$–$C_3$ | 1.402 | 1.380 | 1.377 |
| $C_2$–$S_1$ | 1.707 | 1.746 | 1.731 |
| $C_3$–$C_4$ | 1.410 | 1.416 | 1.411 |
| $C_4$–$C_5$ | 1.340 | 1.371 | 1.370 |
| $C_5$–$S_1$ | 1.689 | 1.723 | 1.710 |
| *Bağ Angles (°)* | | | |
| $C_{12}$–$C_{11}$–$C_{10}$ | 120.5 | 120.0 | 120.0 |
| $C_{12}$–$C_{11}$–$Cl_{16}$ | 119.1 | 119.8 | 119.8 |
| $C_{10}$–$C_{11}$–$Cl_{16}$ | 120.4 | 120.0 | 120.1 |
| $C_{13}$–$C_{12}$–$C_{11}$ | 121.2 | 120.8 | 120.7 |
| $C_{13}$–$C_{12}$–$Cl_{18}$ | 118.3 | 117.8 | 118.0 |
| $C_{14}$–$C_{13}$–$C_{12}$ | 118.1 | 118.8 | 118.9 |
| $C_{15}$–$C_{14}$–$C_{13}$ | 122.2 | 121.2 | 121.1 |
| $C_{15}$–$C_{14}$–$Cl_{19}$ | 118.8 | 119.6 | 119.6 |
| $C_{13}$–$C_{14}$–$Cl_{19}$ | 119.0 | 119.1 | 119.1 |
| $C_{14}$–$C_{15}$–$C_{10}$ | 120.3 | 120.6 | 120.5 |
| $C_{11}$–$C_{10}$–$C_{15}$ | 117.7 | 118.3 | 118.5 |
| $C_{11}$–$C_{10}$–$C_9$ | 121.2 | 121.1 | 120.9 |
| $C_{15}$–$C_{10}$–$C_9$ | 121.0 | 120.4 | 120.4 |
| $C_9$–$C_8$–$C_6$ | 121.4 | 120.3 | 119.8 |
| $O_7$–$C_6$–$C_2$ | 120.6 | 120.7 | 120.7 |
| $O_7$–$C_6$–$C_8$ | 122.1 | 121.7 | 121.9 |
| $C_2$–$C_6$–$C_8$ | 117.3 | 117.4 | 117.3 |
| $C_3$–$C_2$–$C_6$ | 129.8 | 130.8 | 130.8 |
| $C_3$–$C_2$–$S_1$ | 110.9 | 110.8 | 110.9 |
| $C_6$–$C_2$–$S_1$ | 119.3 | 118.3 | 118.1 |
| $C_2$–$C_3$–$C_4$ | 111.0 | 113.2 | 112.9 |
| $C_5$–$C_4$–$C_3$ | 113.2 | 112.2 | 112.0 |
| $C_4$–$C_5$–$S_1$ | 112.9 | 112.5 | 112.5 |
| $C_5$–$S_1$–$C_2$ | 92.0 | 91.2 | 91.4 |

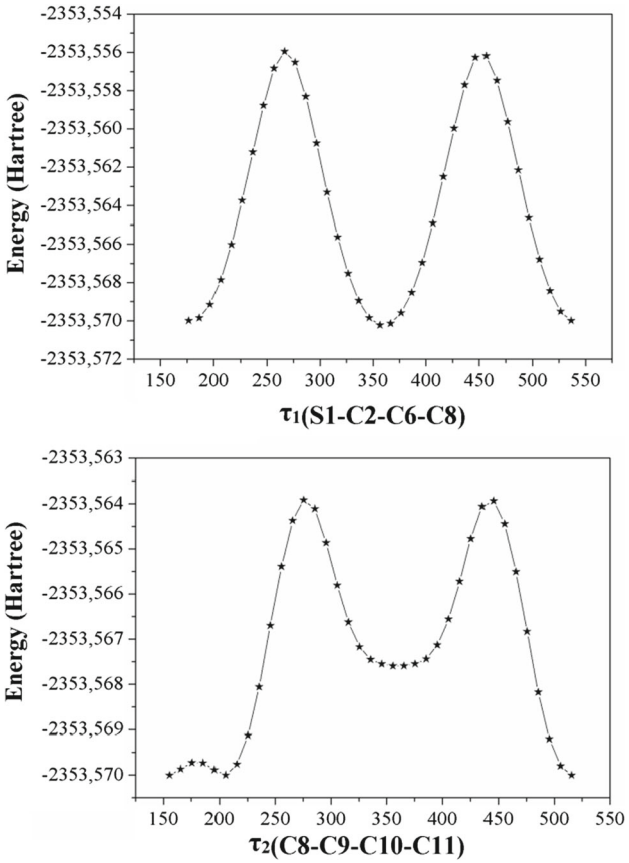


**Fig. 2** PES scans of energy and dihedral angles for the TTCP

## 3.2 Potential Energy Surface (PES) Scan

A conformational study is done to determine stable conformers. These stable conformers are called sampling points on PES (potential energy surface). The sampling points are important to determine the minimum energy conformation to obtain data about the structure of the protein. The simple points found in scanning for the TTCP are calculated with the B3LYP method at the minimum energy level. To find possible conformation of the TTCP, the potential energy curve is calculated between 0° and 360° in 10° steps. Confirmation of the TTCP was calculated for $\tau_1$ ($S_1$–$C_2$–$C_6$–$C_8$) and $\tau_2$ ($C_8$–$C_9$–$C_{10}$–$C_{11}$) dihedral angles. PES scan of the TTCP is shown in Fig. 2. Stable minimum point was observed 365.472° at − 2353.570 Hartree energy value for $\tau_1$($S_1$–$C_2$–$C_6$–$C_8$) dihedral angle and 205.472° at − 2353.570 Hartree energy value for $\tau_2$ ($C_8$–$C_9$–$C_{10}$–$C_{11}$) dihedral angle. There are two maximum points on PES, global and local. The two maximum points of $\tau_1$($S_1$–$C_2$–$C_6$–$C_8$) dihedral are 266.503° and 456.503° at − 2353.556 Hartree energy value. The two maximum points of $\tau_2$ ($C_8$–$C_9$–$C_{10}$–$C_{11}$) dihedral are 275.472° and 445.472° at − 2353.564 Hartree energy value. 3D contour potential surface graph of the TTCP shown in Fig. 3 for $S_1$–$C_2$–$C_6$–$C_8$

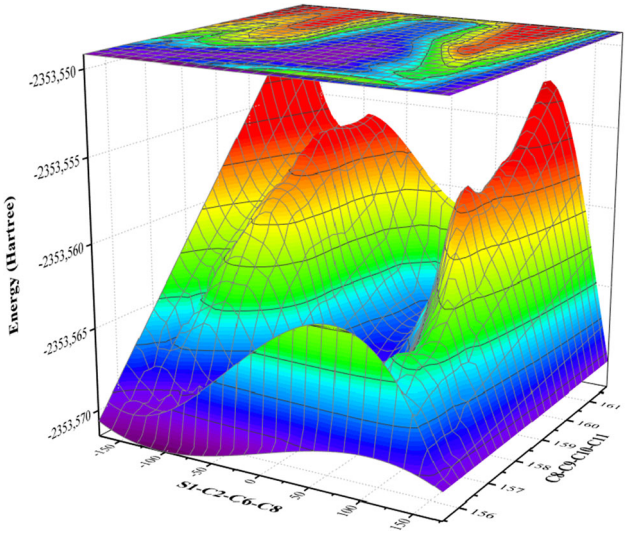


**Fig. 3** 3D Contour graphic of molecular energy surfaces for the TTCP

and $C_8$–$C_9$–$C_{10}$–$C_{11}$ dihedral angles.

### 3.3 IR Spectra

To better understand the spectral properties of the TTCP, theoretical vibration modes were studied in detail. Theoretical vibration assignments and functional groups are summarized in Table 2. Optimized structural data are used to calculate vibrational wavenumbers. As seen in Table 2, the absence of negative vibration wavenumber verified that the optimized structure is stable. The DFT method underestimates interactions such as intermolecular hydrogen bonds and considers molecules. Since theoretical and experimental data to be more compatible with each other, it is essential to multiply by the 0.9614 coefficient [24–26].

Experimental stretching bands (C–H) were observed at 3062, 2967, and 2812 (in $cm^{-1}$) [1]. Theoretical C–H stretching bands were calculated in the range of 3114–3079 (in $cm^{-1}$) for the B3LYP method and 3135–3101 $cm^{-1}$ for the HSEh1PBE method. C–H in-plane bending vibrations appear as a very weak peak in the frequency region 1000–1550 $cm^{-1}$ [27]. These peaks were found at 1540–1042 and 1569–1051 $cm^{-1}$ mostly coupled peaks with the PED contribution of 15–49%. It is reported that the bands at the range of 1400 and 1650 $cm^{-1}$ in the aromatic and heteroaromatic compounds are assigned to the C–C bond vibrations [28]. According to Varsanyi [26], these bands have variable intensity observed at 1625–1280 (in $cm^{-1}$). C–C stretching vibrations were calculated at 1643–1021 (in $cm^{-1}$) for the B3LYP method and 1676–1035 $cm^{-1}$ for the HSEh1PBE method. Manjunath et al. reported that the peak was observed at 1591 $cm^{-1}$ from the C=C stretching vibrations [1]. This peak is calculated at 1581 and 1613 $cm^{-1}$

**Table 2** Experimental and theoretical vibrational wavenumbers and assignments for the TTCP

| Assignments with B3LYP PED%[a] | FT-IR [1] | B3LYP scaled freq.[b] | HSEh1PBE Scaled freq.[b] |
|---|---|---|---|
| ν CH 82 (T) | | 3114 | 3135 |
| ν CH 72 (B) | | 3095 | 3115 |
| ν CH 69 (T) | | 3094 | 3112 |
| ν CH 59 (B) | | 3089 | 3105 |
| ν CH 69 (T) | | 3079 | 3101 |
| ν CH 64 | | 3063 | 3080 |
| ν CH 66 | | 3057 | 3070 |
| ν CO 12 + ν CC 14 | 1649 | 1643 | 1676 |
| ν CO 9 + ν CC 25 | 1591 | 1581 | 1613 |
| ν CC 31 (B) + β CCH 17 (B) | | 1540 | 1569 |
| ν CC 17 (B) | | 1516 | 1546 |
| ν CC 20 (T) + β CCH 20 (T) | | 1495 | 1516 |
| ν CC 28 (T) + β CCH 28 (T) | | 1395 | 1420 |
| β CCH 15 (B) | | 1380 | 1398 |
| ν CC 22 (B) + β CCH 18 (B) | | 1366 | 1384 |
| ν CC 16 (T) + β CCH 24 (T) | | 1329 | 1342 |
| β CCH 29 | | 1299 | 1309 |
| β CCH 22 | | 1280 | 1290 |
| ν CC 24 (B) | | 1233 | 1260 |
| β CCH 38 (T) | | 1207 | 1209 |
| β CCH 27 | | 1177 | 1187 |
| ν CC 6 (B) + ν CCl 6 (B) | | 1153 | 1168 |
| ν CC 15 (B) + ν CCl 11 (B) | | 1097 | 1106 |
| ν CC 6 (T) + β CCH 45 (T) + β SCH 17 (T) | | 1064 | 1064 |
| ν CC 14 (T) + β CCH 49 (T) | | 1042 | 1051 |
| ν CC 16(B) | | 1021 | 1035 |
| τ HCCH 17 + τ CCCC 12 + τ CCCH 23 | | 977 | 978 |
| τ SCCH 10 + τ HCCH 34 + τ CCCH 13 | | 885 | 888 |
| τ SCCH 12 + τ HCCH 10 + τ CCCH 18 | | 812 | 816 |
| ν CCl 14 (B) | 720 | 792 | 798 |
| ν SC 27 (T) | 676 | 717 | 735 |

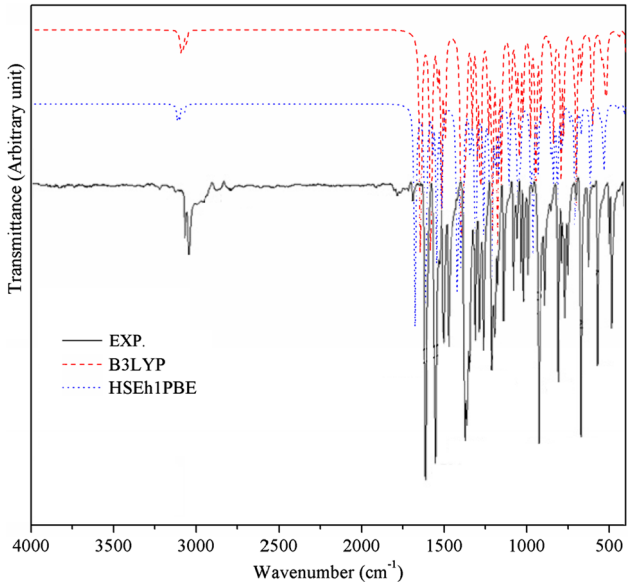


**Fig. 4** Calculated and observed IR spectra for the TTCP

with a PED contribution of 25%, respectively. The stretching vibration (C=O) [29, 30] is observed in the region 1715–1680 (in $cm^{-1}$). The strong peak appeared at 1649 $cm^{-1}$ assigned as C=O stretching vibration [1]. This peak is found at 1643 and 1581 $cm^{-1}$ for B3LYP method, 1676 and 1613 $cm^{-1}$ for HSEh1PBE method with the PED contribution of 12–9%. This mode is coupled with the C=C stretching vibrations. Because the large degree of their $\pi$-electron delocalization is insufficient due to conjugation of the molecule, the number of waves is calculated for this mode deviates. The assignments of C–S bands are a rough task in thiophenes due to the shorter bond length and higher polarity of the C–S bond in thiophenes [31]. This mode is observed at the range of 872–750 $cm^{-1}$ [32]. Manjunath et al. reported the band at 676 $cm^{-1}$ originated from C–S stretching vibration [1]. This mode is calculated at 717 and 735 (in $cm^{-1}$) for B3LYP and HSEh1PBE methods, respectively. For simple organic chlorine compounds, C–Cl absorptions in the region were 750–700 $cm^{-1}$ [33, 34]. In the TTCP, the peak was observed at 720 $cm^{-1}$ [1] and calculated at 792 and 798 $cm^{-1}$. The experimental and theoretical IR spectra for the TTCP molecule are shown in Fig. 4.

## 3.4 Natural Bonding Orbital

Natural Bonding Orbital (NBO) method examines charge conjugative or transfers interactions in molecular systems [35]. The method performs it possible to study hyper conjugative interactions due to electron transitions between acceptor–donor orbitals. From donor–acceptor, more electrons increase conjugation and stabilization energy of the system.

NBO results are listed in Table 3. According to Table 3, LP2 ($O_7$) $\rightarrow \sigma^*$ ($C_2$–$C_6$) and LP3 ($C_{19}$) $\rightarrow \pi^*$ ($C_{14}$–$C_{15}$) interaction energies are found 17.91 and 12.76 kcal/mol at the B3LYP level. A number of the same types of interactions are calculated for the TTCP. The intramolecular hyper conjugative interaction of $\sigma$ ($C_{10}$–$C_{11}$) deploys to $\sigma^*$ ($C_{10}$–$C_{15}$), $\sigma^*$ ($C_{11}$–$C_{12}$) leading to stabilization of 3.13 and 4.15 kcal/mol, respectively. Antibonding orbitals increase conjugation for $\pi^*$ ($C_{15}$–$C_{14}$) and $\pi^*$ ($C_{12}$–$C_{13}$) which provides strong delocalization of 18.68 and 20.88 kcal/mol, respectively. Interaction energies of LP1 $S_1 \rightarrow \sigma^*$ ($C_3$–$C_2$) and $\sigma$ ($C_6$–$C_8$) $\rightarrow \sigma^*$ ($C_2$–$S_1$) calculated as 2.50, 2.58 kcal/mol for B3LYP method and 3.61, 3.62 kcal/mol for the HSEh1PBE method.

## 3.5 Electronic Properties

The transition of an electron from HOMO (highest occupied orbit) to LUMO (lowest empty orbit) is defined as electronic absorption. Total energies of the frontier molecular orbital of the TTCP were investigated at the B3LYP method and shown in Fig. 5. The energy gap is important in definition electrical transport properties of the molecule [36]. Quantum chemical parameters (as chemical activity, HOMO–LUMO energies and their energy gap ($\Delta E$), hardness ($h$), electronegativity ($c$), and electronic transition energies)were performed with B3LYP and HSEh1PBE methods and calculated values listed in Table 4. HOMO–LUMO values were found as − 7.4300 and − 5.8863 eV at the HSEh1PBE method. $\Delta E$ is an electronic system and charge transfer is more likely to occur in a molecular system with a smaller energy gap. Thus, NLO properties of such systems are generally higher than molecules with a larger energy gap. $\Delta E$ were found as 1.5437 and 1.5674 eV at the HSEh1PBE and the B3LYP methods. These values indicate that intramolecular charge transfer takes place in the TTCP molecule.

The $\chi$ (Electronegativity) and $\eta$ (chemical hardness) were calculated as 6.6640 and 0.7837 (in eV) using HOMO–LUMO values. UV–vis spectra of the TTCP were performed by using the TD-DFT method. The absorption band, experimentally was observed at 324 nm and assigned as $n$–$\pi^*$ transition and found at 326 and 331 nm for the B3LYP and the HSEh1PBE methods. Electronic transition energies, wavelengths, and oscillator strengths for the TTCP are given in Table 4.

## 3.6 Nonlinear Optics

Hyperpolarizability increases in organic molecules containing C=O and C–C groups, which are involved in hydrogen bond interactions. Dipole moment is important to show the motion of intermolecular charge. The dipole moment of the TTCP was found as 4.0438 Debye for the B3LYP method and 3.9950 Debye for the HSEH1PBE method with a maximum

**Table 3** NBO analysis for the TTCP

| Donor (i) | Acceptor (j) | $E(2)^a$ (kcal/mol) | | $E(j) - E(i)^b$ (a.u.) | | $F(i,j)^c$ (a.u.) | |
|---|---|---|---|---|---|---|---|
| | | B3LYP | HSEh1 | B3LYP | HSEh1 | B3LYP | HSEh1 |
| $\sigma$ ($C_3$–$C_2$) | $\sigma^*$ ($C_2$–$C_6$) | 2.53 | 2.74 | 1.19 | 1.20 | 0.05 | 0.05 |
| $\sigma$ ($C_3$–$C_2$) | $\sigma^*$ ($C_6$–$O_7$) | 1.64 | 1.68 | 1.33 | 1.34 | 0.04 | 0.04 |
| $\sigma$ ($C_2$–$S_1$) | $\sigma^*$ ($C_3$–$C_2$) | 0.60 | 0.71 | 1.24 | 1.26 | 0.02 | 0.03 |
| $\sigma$ ($C_2$–$S_1$) | $\sigma^*$ ($C_6$–$C_8$) | 3.09 | 3.10 | 1.09 | 1.11 | 0.05 | 0.05 |
| $\sigma$ ($C_2$–$C_6$) | $\sigma^*$ ($C_6$–$O_7$) | 1.48 | 1.58 | 1.28 | 1.30 | 0.04 | 0.04 |
| $\pi$($C_5$–$C_4$) | $\pi^*$($C_2$–$C_3$) | 17.4 | 16.57 | 0.29 | 0.29 | 0.07 | 0.07 |
| $\pi$($C_2$–$C_3$) | $\pi^*$($C_6$–$O_7$) | 21.0 | 20.26 | 0.30 | 0.30 | 0.07 | 0.07 |
| $\sigma$ ($C_6$–$C_8$) | $\sigma^*$ ($C_2$–$S_1$) | 3.61 | 3.62 | 0.87 | 0.89 | 0.05 | 0.05 |
| $\sigma$ ($C_6$–$C_8$) | $\sigma^*$ ($C_2$–$C_6$) | 1.13 | 1.26 | 1.11 | 1.13 | 0.03 | 0.03 |
| $\sigma$ ($C_6$–$C_8$) | $\sigma^*$ ($C_6$–$O_7$) | 1.13 | 1.23 | 1.25 | 1.26 | 0.03 | 0.04 |
| $\sigma$ ($C_8$–$C_9$) | $\sigma^*$ ($C_{10}$–$C_{11}$) | 2.15 | 2.22 | 1.26 | 1.27 | 0.05 | 0.05 |
| $\pi$ ($C_8$–$C_9$) | $\sigma^*$ ($C_{10}$–$C_{11}$) | 0.56 | 0.54 | 0.79 | 0.80 | 0.02 | 0.02 |
| $\pi$ ($C_8$–$C_9$) | $\pi^*$ ($C_{10}$–$C_{11}$) | 11.6 | 11.54 | 0.28 | 0.27 | 0.06 | 0.05 |
| $\sigma$ ($C_9$–$C_{10}$) | $\sigma^*$ ($C_{10}$–$C_{11}$) | 3.17 | 3.40 | 1.19 | 1.20 | 0.06 | 0.06 |
| $\sigma$ ($C_{10}$–$C_{11}$) | $\sigma^*$ ($C_{10}$–$C_{15}$) | 3.13 | 4.00 | 1.19 | 1.27 | 0.05 | 0.06 |
| $\sigma$ ($C_{10}$–$C_{11}$) | $\sigma^*$ ($C_{11}$–$C_{12}$) | 4.15 | 4.40 | 1.25 | 1.26 | 0.07 | 0.07 |
| $\pi$ ($C_{10}$–$C_{11}$) | $\pi^*$ ($C_{15}$–$C_{14}$) | 18.8 | 17.66 | 0.28 | 0.28 | 0.07 | 0.06 |
| $\pi$ ($C_{10}$–$C_{11}$) | $\pi^*$ ($C_{12}$–$C_{13}$) | 20.9 | 19.56 | 0.28 | 0.27 | 0.07 | 0.07 |
| $\sigma$ ($C_{11}$–$Cl_{16}$) | $\sigma^*$ ($C_{10}$–$C_{15}$) | 2.64 | 2.64 | 1.26 | 1.29 | 0.05 | 0.05 |
| $\sigma$ ($C_{11}$–$Cl_{16}$) | $\sigma^*$ ($C_{12}$–$C_{13}$) | 2.58 | 2.54 | 1.27 | 1.29 | 0.05 | 0.05 |
| LP1 ($S_1$) | $\sigma^*$ ($C_3$–$C_2$) | 2.50 | 2.58 | 1.23 | 1.23 | 0.05 | 0.05 |
| LP1 ($O_7$) | $\sigma^*$ ($C_2$–$C_6$) | 1.88 | 1.86 | 1.14 | 1.15 | 0.04 | 0.04 |
| LP2 ($Cl_{16}$) | $\sigma^*$ ($C_{10}$–$C_{11}$) | 4.51 | 4.80 | 0.84 | 0.84 | 0.06 | 0.06 |
| LP2 ($O_7$) | $\sigma^*$ ($C_2$–$C_6$) | 17.9 | 18.16 | 0.71 | 0.72 | 0.10 | 0.10 |
| LP2 ($O_7$) | $\sigma^*$ ($C_6$–$C_8$) | 19.8 | 19.90 | 0.69 | 0.69 | 0.11 | 0.11 |
| LP3 ($Cl_{19}$) | $\pi^*$ ($C_{14}$–$C_{15}$) | 12.8 | 13.32 | 0.33 | 0.32 | 0.062 | 0.06 |

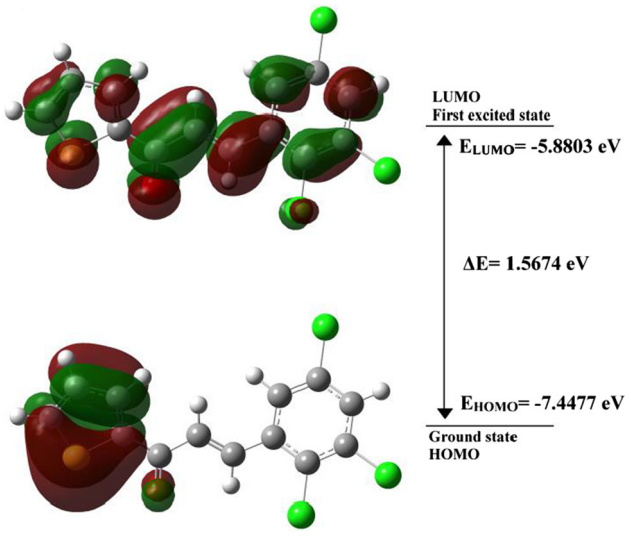


**Fig. 5** The FMOs, HOMO–LUMO energy gap and energies (in eV) for the TTCP

**Table 4** FMOs, energies and calculated physico-chemical properties for the TTCP

| | B3LYP | HSEh1PBE |
|---|---|---|
| $E_{HOMO}$ (eV) | − 7.4477 | − 7.4300 |
| $E_{LUMO}$ (eV) | − 5.8803 | − 5.8863 |
| $\Delta E = E_{LUMO} - E_{HOMO}$ (eV) | 1.5674 | 1.5437 |
| $\chi$(eV) | 6.6640 | 6.6582 |
| $\eta$(eV) | 0.7837 | 0.7719 |

additive from -y-axis (as seen in Table 5). NLO materials are very important for future applications in the optoelectronics field.

Due to hyperpolarizability, organic materials have non-linear optic features. Organic, Inorganic, and organometallic molecular systems are investigated for NLO active feature. $\mu$ (total static dipole moment), $< \alpha >$ (the mean polarizability), $\Delta\alpha$ (the anisotropy of the polarizability) and $< \beta >$ (the

**Table 5** The electric dipole (hyper) polarizabilities for the TTCP

| Property | B3LYP | HSEh1PBE |
|---|---|---|
| $\mu_x$ | − 1.2835 | − 1.2182 |
| $\mu_y$ | 3.6017 | 3.5842 |
| $\mu_z$ | 1.3161 | 1.2766 |
| $\mu$ | 4.0438 | 3.9950 |
| $\alpha_{xx}$ | 51.776 | 50.846 |
| $\alpha_{yy}$ | 35.093 | 34.515 |
| $\alpha_{zz}$ | 17.800 | 17.396 |
| $<\alpha>$ | 34.890 | 34.252 |
| $\Delta\alpha$ | 29.426 | 28.972 |
| $\beta_x$ | − 1.308 | − 2.446 |
| $\beta_y$ | − 4.206 | − 3.949 |
| $\beta_z$ | − 2.945 | − 3.068 |
| $<\beta>$ | 5.299 | 5.567 |

mean first-order hyperpolarizability) parameters were performed using defined equations previously [37]. All NLO parameters ($<\alpha>$, $\Delta\alpha$ and $<\beta>$) were calculated with the B3LYP and the HSEh1PBE methods for the TTCP. $<\alpha>$, $\Delta\alpha$ and $<\beta>$ parameters in Gaussian output file were calculated in atomic units. Calculated $<\alpha>$, $\Delta\alpha$ and $<\beta>$ values were converted to electrostatic units ($\alpha$: 1 a.u. = $0.1482 \times 10^{-24}$ esu. and $\beta$: 1 a.u. = $8.6393 \times 10^{-33}$ esu.). Calculated $<\alpha>$, $\Delta\alpha$ and $<\beta>$ were found as $29.426 \times 10^{-24}$, $34.890 \times 10^{-24}$ and $5.299 \times 10^{-30}$ esu. at B3LYP method for the TTCP. Calculated maximum $\beta$ data ($\beta y$) is due to $\pi$–$\pi$ interactions and hydrogen bonds. Calculated maximum $\beta$ data show that the electron cloud is more in the y-direction.

### 3.7 Molecular Surfaces and Atomic Charge Analysis

Molecular surfaces are a technique of mapping electrostatic potential onto the iso-electron density surface. MEP surface map is very important for the investigation of molecular structure. MEP surface map shows the molecule's color, shape, charge, size, and electrostatic potential regions at the same time. The color chart of MEP is red for (−) charge, blue for (+) charge, yellow for the slightly electron-rich region, green for neutral [38]. 3D MEPs of the TTCP were simulated by using the B3LYP and shown in Fig. 6. The electrolyte will hold from oxygen atom to the TTCP, as seen in Fig. 6.

Unlike electron density, atomic charges cannot be observed quantum mechanically, so they cannot be calculated exactly. Developed methods contain randomness for calculating this quantity. Mulliken charge distribution is an old method and common method [39]. This method is a linear combination of atomic orbital results based on the method of obtaining molecular orbital. In case making the distribution to atoms of wave functions, it is based on the principle

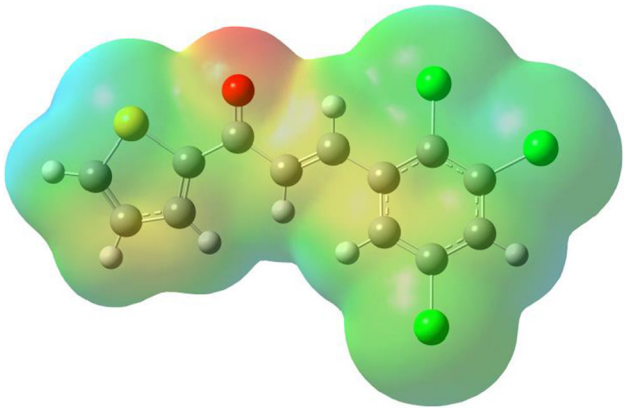

**Fig. 6** MEP surface plots for the TTCP

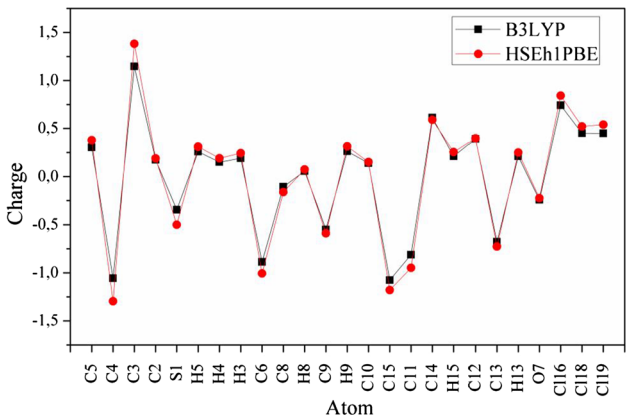


**Fig. 7** Comparative of Mulliken atomic charges for the TTCP

of equally distributing two overlapping orbits. The B3LYP and the HSEh1PBE methods are used to calculating atomic charges of the TTCP. Calculated Mulliken density analysis results are shown in Fig. 7. The magnitude of C charges is given to be either (+) or (−) are recorded to change from − 1.07543 to 1.14634 with the B3LYP method.

### 3.8 Molecular Docking Analysis

Molecular interactions play important roles in the basic biological processes. These molecular interactions lead to the formation of stable ligand–protein complexes that are necessary for their biological functions. Molecular docking was performed by AutoDock (version 4.0) program. The program receives a semi empirical free energy force in docking simulation processes. The force field contains (Vi) and a loss of conformational entropy after binding (ΔSconf):

$$\Delta G = (V_{\text{bound}}^{L-L} - V_{\text{unbound}}^{L-L}) + (V_{\text{bound}}^{P-P} - V_{\text{unbound}}^{P-P}) + (V_{\text{bound}}^{P-L} - V_{\text{unbound}}^{P-L} + \Delta S_{\text{conf}})$$

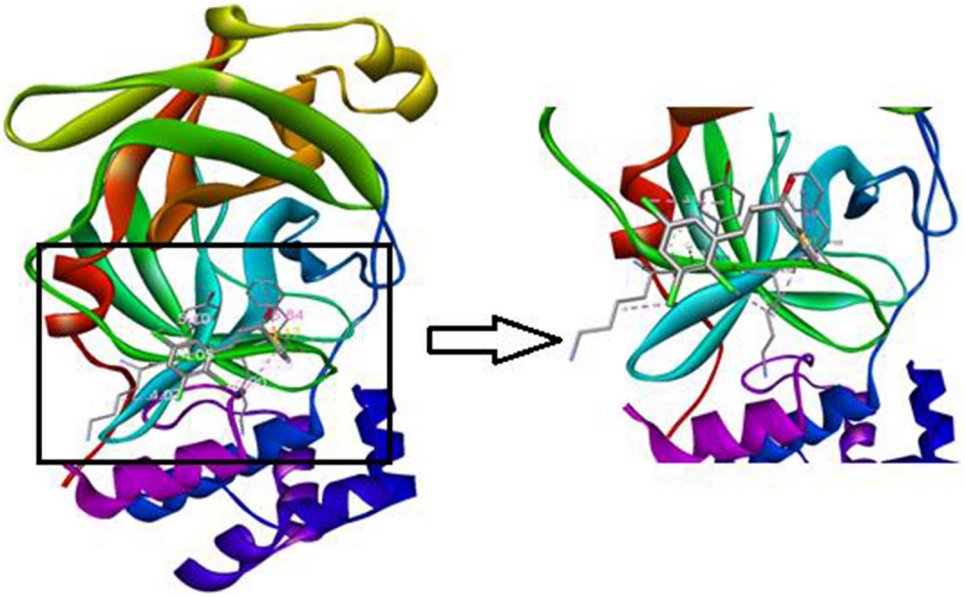

**Fig. 8** The 3D interaction diagrams of the TTCP in into the active sites PDB 5R7Y main protease

where L refers to the ligand and P to the protease [40]. The PDB 5R7Y target protease exhibits the minimum binding energy of − 4.12 kcal/mol, intermolecular energy of − 4.47 kcal/mol, and an inhibition constant of 959.73 micromolar (uM). The deviation between the ligand- protease was analyzed, where the root mean square deviation (RMSD) value was calculated as 24.21 for TTCP molecule.

3D molecular interaction diagrams of target protease (PDB 5R7Y) and ligand (TTCP) are shown in Fig. 8. Detailed 2D interaction diagrams are shown in Fig. 9. The molecular docking results show that the analyzed TTCP molecule has a 2 pi-anion interactions with the A100 residue of PDB 5R7Y, which is characterized by interaction lengths of 4.07 Å. The TTCP molecule and the target have PDB 5R7Y C•••O interaction and pi-alkyl interaction in the range of 4.90–5.29 Å interaction length. With the TTCP molecule, the target PDB 5R7Y has a sulfur-x interaction with residue A103, which is characterized by interaction lengths of 3.17 A, and also has a pi-donor hydrogen interaction with residue A101 with an interaction length of 4.05 Å. The total energy of the best conformation obtained for the TTCP complex was calculated as 4.12 kcal/mol, and the inhibition constant was calculated as 959,73um (micromolar). According to this docking result, the TTCP molecule appears to be active with PDB 5R7Y.

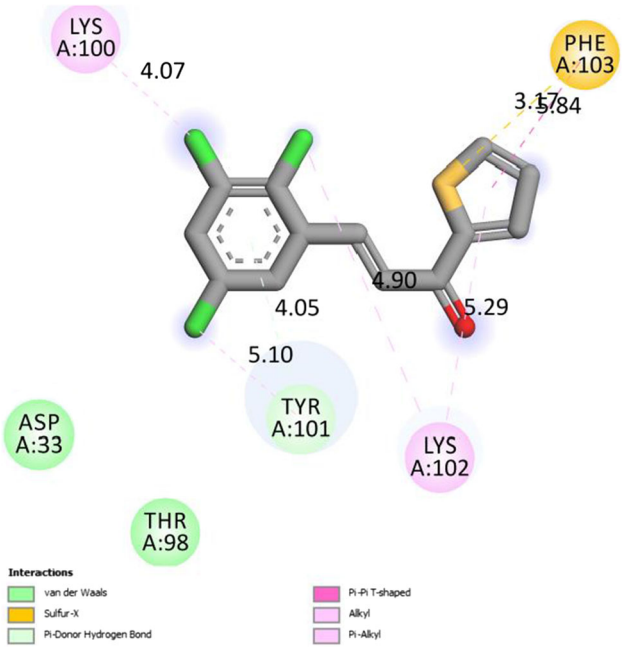


**Fig. 9** The binding orientation and 2D molecular interaction diagram of the TTCP in into the active sites of PDB 5R7Y main protease

## 4 Conclusions

The 1-(2´-Thiophen)-2-propen-1-one-3-(2,3,5-trichlorophenyl) (TTCP) molecule from thiophene-containing compounds were investigated as inhibitors for COVID-19 with help of DFT and molecular docking calculations. Molecular Modeling of the TTCP molecule was done by using Gaussian 09 W program. Firstly, the molecular geometry of the TTCP molecule was optimized with DFT/B3LYP and DFT/HSEH1PBE methods using 6–311++ G(d,p) basis set. Detailed assignments of vibration modes were shown using PED (potential energy distribution). UV–vis spectrum inspected for optimized the TTCP. Optimized geometric parameters (bond lengths and angles), vibration and UV–vis spectra theoretical data were observed in accordance with the experimental data. Additionally, 3D potential energy surface was investigated

for S1–C2–C6–C8 and C8–C9–C10–C11 dihedral angles, and the fixed points are minimally verified by the frequency analysis. According to the potential energy surface scan calculations, the energy value of most stable structure which located on the global minimum point is − 2353.570 Hartree for $\tau_1$(S1–C2–C6–C8). The HOMO–LUMO energy band gap for the TTCP molecule was calculated as 1.5674 eV at B3LYP method. This low energy band gap indicates that it supports the bioactive property of the TTCP molecule.

The reactivity of the TTCP molecule in the treatment of coronavirus by combining DFT and molecular docking calculations were determined. As a result of DFT and molecular docking analyses, TTCP molecule is suggested as a potential antiviral for the treatment of Covid-19 diseases. The interactions between ligand-target were examined by using molecular docking and it was observed that TTCP molecule is a good inhibitor of COVID-19 virus. According to the docking results, the TTCP molecule can be effective in the control of COVID-19 disease has contributed to the literature.

## References


1. Manjunath, H.R.; Kumar, P.R.; Naveen, S.; Ravindrachary, V.; Sridhar, M.A.; Prasad, J.S.; Karegoudar, P.: Growth, characterization, crystal and molecular structure studies of 1-(2′-thiophen)-3-(2, 3, 5-trichlorophenyl)-2-propen-1-one. J. Crystal Growth **327**(1), 161–166 (2011). https://doi.org/10.1016/j.jcrysgro.2011.06.006
2. Huang, W.; Yu, W.L.; Meng, H.; Pei, J.; Li, S.F.Y.: New series of blue-light-emitting polymers constituted of 3-alkylthiophenes and 1, 4-di (1, 3, 4-oxadiazolyl) phenylene. Chem. Mater. **10**(11), 3340–3345 (1998). https://doi.org/10.1021/cm9800581
3. Blumstengel, S.; Sokolik, I.; Dorsinville, R.; Voloschenkob, D.; Heb, M.; Lavrentovichb, O.; Chienb, L.C.: Photo-, and electroluminescence studies of 2,5-bis[2′-(4″-(6-hexoxy benzyl))-1′-ethenyl]-3, 4-dibutyl thiophenes. Chien. Synth. Met. **99**, 85–90 (1999). https://doi.org/10.1016/S0379-6779(98)01492-1
4. Batista, R.M.F.; Costa, S.P.G.; Belsley, M.; Manuela, M.; Raposo, M.: Synthesis and optical properties of novel, thermally stable phenanthrolines bearing an arylthienyl-imidazo conjugation pathway. Dyes Pigments **80**, 329–336 (2009). https://doi.org/10.1016/j.dyepig.2008.08.001
5. Hosmane, R.S.; Liebman, J.F.: Aromaticity of heterocycles: experimental realization of dewar-breslow definition of aromaticity. Tetrahedron Lett. **32**, 3949–3952 (1991). https://doi.org/10.1016/0040-4039(91)80597-Y
6. Lin, J.W.P.; Dudek, L.P.: Synthesis and properties of poly (2, 5-thienylene). J. Polym. Sci. Polym. Chem. Ed. **18**(9), 2869–2873 (1980). https://doi.org/10.1002/pol.1980.170180910
7. Jen, K.Y.; Miller, G.G.; Elsenbaumer, R.L.: Highly conducting, soluble, and environmentally-stable poly(3-alkylthiophenes). J. Chem. Soc. Chem. Commun. **17**, 1346–1347 (1986). https://doi.org/10.1039/C39860001346
8. Hu, X.; Xu, L.: Structure and properties of 3-alkoxy substituted polythiophene synthesized at low temperature. Polymer **41**(26), 9147–9154 (2000). https://doi.org/10.1016/S0032-3861(00)00299-8
9. Frisch, M.J., et al.: Fox, Gaussian 09, Revision A.1. Gaussian Inc., Wallingford CT (2009)
10. GaussView, V.: 5, Roy Dennington, Todd Keith, John Millam. Semichem Inc., Shawnee Mission KS (2009)
11. Becke, A.D.: J. Chem. Phys. **98**, 5648 (1993). https://doi.org/10.1063/1.464913
12. Lee, C.; Yang, W.; Parr, R.G.: Development of the Colle-Salvetti correlation-energy formula into a functional of the electron density. Phys. Rev. B **37**(2), 785 (1988). https://doi.org/10.1103/PhysRevB.37.785
13. Heyd, J.; Scuseria, G.E.: Efficient hybrid density functional calculations in solids: assessment of the Heyd–Scuseria–Ernzerhof screened Coulomb hybrid functional. J. Chem. Phys. **121**(3), 1187–1192 (2004). https://doi.org/10.1063/1.1760074
14. Heyd, J.; Scuseria, G.E.: Assessment and validation of a screened Coulomb hybrid density functional. J. Chem. Phys **120**(16), 7274–7280 (2004). https://doi.org/10.1063/1.1668634
15. Heyd, J.; Peralta, J.E.; Scuseria, G.E.; Martin, R.L.: Energy band gaps and lattice parameters evaluated with the Heyd-Scuseria-Ernzerhof screened hybrid functional. J. Chem. Phys. **123**(17), 174101 (2005). https://doi.org/10.1063/1.2085170
16. Heyd, J.; Scuseria G.E.J. Chem. Phys. **124**, 219906 (2006). https://doi.org/10.1063/1.2204597
17. Frisch, M.J.; Pople, J.A.; Binkley, J.S.: Self-consistent molecular orbital methods 25. Supplementary functions for Gaussian basis sets. J. Chem. Phys. **80**(7), 3265–3269 (1984). https://doi.org/10.1063/1.447079
18. Michalska, D.: Raint program. Wroclaw University of Technology, (2003)
19. http://www.rcsb.org/
20. Sanner, M.F.: Python: a programming language for software integration and development. J. Mol. Graph. Model. **17**, 57–61 (1999)
21. De Lano, W.L.: The PyMOL Molecular Graphics System. San Carlos, CA, De Lano Scientific (2004)
22. Morris, G.M.; Huey, R.; Lindstrom, W.; Sanner, M.F.; Belew, R.K.; Goodsell, D.S.; Olson, A.J.: AutoDock4 and AutoDockTools4: automated docking with selective receptor flexibility. J. Comput. Chem. **30**, 2785–2791 (2009). https://doi.org/10.1002/jcc.21256
23. Dassault Syst_emes BIOVIA DiscoveryStudio Modeling Environment. Release 2017 Dassault Systemes, 2016.
24. Frish, A.; Nielsen, A.B.; Holder, A.J.: Gauss View User Manual. Gaussian Inc., Pittsburg, PA (2001)
25. Eşme, A.: Spectroscopic calculations, Hirshfeld surface analysis, and molecular docking studies of anticancer 6-(4-Aminophenyl)-4-(4-methoxyphenyl)-2-methoxynicotinonitrile. Spect. Lett. **54**, 51–64 (2021). https://doi.org/10.1080/00387010.2020.1845213
26. Varsanyi, G.: vols. 1–2. Adam Hilger, (1974)
27. Gümüş, H.P.: Conformational, spectroscopic, electric and electronic investigations on 5-nitropyridine-2-hydrazino-3-carbonitrile-6-methyl-4-(methoxymethyl) (molecule 2): molecular docking study. J. Mol. Struct. **1211**, 128018 (2020). https://doi.org/10.1016/j.molstruc.2020.128018
28. Abdelbassit, M.S.; Popoola, S.A.; Saleh, T.A.; Abdallah, H.H.; Al-Saadi, A.A.; Alhooshani, K.R.: DFT and kinetic evaluation of chloromethane removal using cost-effective activated carbon. Arab. J. Sci. Eng. **45**, 4705–4716 (2020). https://doi.org/10.1007/s13369-020-04458-x
29. Roeges, N.P.G.: Wiley, New York (1994)
30. Pakdel, L.; Sedghamiz, T.; Azami, S.M.: DFT Study of the Interaction of Trialkylamines with Ni4-Clusters. Arab. J. Sci. Eng. **44**, 199–208 (2019). https://doi.org/10.1007/s13369-018-3420-y
31. Özdemir, M.; Köksoy, B.; Ceyhan, D.; Sayın, K.; Erçağ, E.; Bulut, M.; Yalçın, B.: Design and in silico study of the novel coumarin derivatives against SARS-CoV-2 main enzymes. J. Biomol. Struct. Dyn. **40**(11), 4905–4920 (2022). https://doi.org/10.1080/07391102.2020.1863263

32. Klots, T.D.; Chirico, R.D.; Steele, W.V.: Complete vapor phase assignment for the fundamental vibrations of furan, pyrrole and thiophene. Spectrochim. Acta A. **50**, 765–795 (1994)
33. Özdemir, M.; Köksoy, B.; Ceyhan, D.; Sayın, K.; Erçağ, E.; Bulut, M.; Yalçın, B.: In silico, 6LU7 protein inhibition using dihydroxy-3-phenyl coumarin derivatives for SARS-CoV-2. J. Turk. Chem. Soc. Sect. A Chem. **7**, 691–712 (2020). https://doi.org/10.18596/jotcsa.753157
34. Ramalingam, S.; Periandy, S.: Vibrational spectroscopy [FTIR and Raman] investigation, computed vibrational frequency analysis and IR intensity and Raman activity peak resemblance analysis on 4-chloro 2-methylaniline using HF and DFT [LSDA, B3LYP and B3PW91] calculations. Spectrochim. Acta Part A **78**, 1149–1161 (2011). https://doi.org/10.1016/j.saa.2010.12.068
35. Gümüş, H.: Spectroscopic (Vibrational and NMR) Characterizations and Molecular Docking Analysis of Zn (II), Cd (II) and Hg (II) Complexes with Alkyl-Aryl Dithiocarbamates. Arab. J. Sci. Eng. **45**(6), 4929–4937 (2020). https://doi.org/10.1007/s13369-020-04358-0
36. Fukui, K.: Role of frontier orbitals in chemical reactions. Science **218**(4574), 747–754 (1982)
37. Maroulis, G.: Static hyperpolarizability of the water dimer and the interaction hyperpolarizability of two water molecules. J. Chem. Phys. **113**, 1813 (2000). https://doi.org/10.1063/1.481985
38. Pir, H.; Günay, N.; Avcı, D.; Tamer, Ö.; Tarcan, E.; Atalay, Y.: Theoretical Investigation of 6-(3, 3, 4, 4, 4-Pentafluoro-2-Hydroxy-1-Butenyl)-2, 4-Dimethoxy-Pyrimidine Molecule. Arab. J. Sci. Eng. **39**(7), 5799–5814 (2014). https://doi.org/10.1007/s13369-014-1131-6
39. Mulliken, R.S.: J. Chem. Phys. **23**, 1833 (1955). https://doi.org/10.1063/1.1740588
40. Reed, A.E.; Weinhold, F.: Natural localized molecular orbitals. J. Chem. Phys. **83**, 1736 (1985). https://doi.org/10.1063/1.449360